**Aalborg Universitet**

# Evaluation of predicted knee function for component malrotation in total knee arthroplasty

Vanheule, Valentine; Delport, Hendrik Pieter; Andersen, Michael Skipper; Scheys, Lennart; Wirix-Speetjens, Roel; Jonkers, Ilse; Victor, Jan; Vander Sloten, Jos

1  **1. Title page**

2

# Evaluation of predicted knee function for component malrotation in total knee arthroplasty

6

7  Valentine Vanheule[a,b], Hendrik Pieter Delport[c], Michael Skipper Andersen[d], Lennart Scheys[c],
8  Roel Wirix-Speetjens[b], Ilse Jonkers[e], Jan Victor[f] and Jos Vander Sloten[a]

9
10  [a]Biomechanics section, Katholieke Universiteit Leuven, Celestijnenlaan 300C, 3001 Leuven, Belgium
11  [b]Materialise N.V., Technologielaan 15, 3001 Leuven, Belgium
12  [c]Department of Orthopaedics, University Hospital Pellenberg, Katholieke Universiteit Leuven, Weligerveld 1, 3212
13  Pellenberg, Belgium
14  [d]Department of Mechanical and Manufacturing Engineering, Aalborg University, Fredrik Bajers Vej 5, 9100 Aalborg,
15  Denmark
16  [e]Department of Kinesiology, Katholieke Universiteit Leuven, Tervuursevest 101, 3001 Leuven, Belgium
17  [f]Department of Physical Medicine and Orthopedic Surgery, Ghent University, De Pintelaan 185, 9000 Ghent, Belgium

18

19

20

21

22

23

24

25

26  **Corresponding author**

27  Valentine Vanheule

28
29  Department of Mechanical Engineering
30  Division BMe
31  Celestijnenlaan 300C
32  3001 Leuven, Belgium
33  valentine.vanheule@kuleuven.be

34  Phone: +32 16 74 42 71
35  Fax: +32 16 39 66 00

36

## 2. Abstract

Soft-tissue balancing for total knee arthroplasty (TKA) remains subjective and highly dependent on surgical expertise. Pre-operative planning may support the clinician in taking decisions by integrating subject-specific computer models that predict functional outcome. However, validation of these models is essential before they can be applied in clinical practice. The aim of this study was to evaluate a knee modelling workflow by comparing experimental cadaveric measures to model-based kinematics and ligament length changes. Subject-specific models for three cadaveric knees were constructed from medical images. The implanted knees were mounted onto a mechanical rig to perform squatting, measuring kinematics and ligament length changes with optical markers and extensometers. Coronal malrotation was introduced using tibial inserts with a built-in slope. The model output agreed well with the experiment in all alignment conditions. Kinematic behaviour showed an average RMSE of less than 2.7 mm and 2.3° for translations and rotations. The average RMSE was below 2.5% for all ligaments. These results show that the presented model can quantitatively predict subject-specific knee behaviour following TKA, allowing evaluation of implant alignment in terms of kinematics and ligament length changes. In future work, the model will be used to evaluate subject-specific implant position based on ligament behaviour.

## 3. Introduction

Creating appropriate soft-tissue balance during total knee replacement surgery is mainly subjective and highly dependent on the surgeon's expertise [1,2]. Pre-operative planning incorporating predictive tools to evaluate functional outcome may support the surgeon by comparing different surgical treatments. Subject-specific musculoskeletal models have a high potential to be used as a predictive tool in clinical practice [3]. In detailed joint models, ligaments strongly influence kinematics since they are highly important structures for guiding and stabilising knee motion [4,5]. However, before applying such models in a clinical setting, validation is of paramount importance. The purpose of this study was to evaluate a computational efficient model that can predict subject-specific knee kinematics and ligament length changes for different implant alignments.

Recently, several studies explored methods that can simultaneously compute motions as well as muscle and contact forces. Hast and Piazza presented a dual-joint workflow in which the knee joint is alternated between a simplified knee joint representation for inverse dynamics and an unconstrained knee with elastic foundation contact [6]. Thelen et al. extended the computed muscle control algorithm (CMC) to co-simulate muscle and contact forces, using an elastic foundation model [7]. Guess et al. presented a two-stage modelling method, an inverse kinematics and a forward dynamics simulation, predicting muscle and contact forces concurrently [8].

Andersen et al. introduced an alternative approach, called force-dependent kinematics (FDK), that extends the fast inverse dynamic simulations with the ability to estimate secondary joint kinematics [9]. This method relies on an assumption of quasi-static force equilibrium in the secondary joint kinematics at each time step during the analysis. In 2014, the FDK method was applied and knee contact forces were validated during walking activities in the winning model of the Grand Challenge competition [10].

86 Musculoskeletal models have the ability to explore the relationship between implant alignment

87 and functional outcome for different activities of daily living. Others investigated the effects of

88 implant alignment variation during a simulated squat, however, without collecting experimental

89 evidence for the malaligned configurations [11,12]. In our study, we modelled different implant

90 alignment variations and additionally, performed a cadaveric study to validate the predicted

91 knee function for each alignment. FDK was used to simulate knee kinematics and predict

92 ligament length change patterns for three cadaveric knees with TKA performing a squat motion.

93 In addition to the standard implant, malrotation in the coronal plane was introduced by using

94 tibial inserts with a built-in varus or valgus offset [13]. For each specimen, three squats were

95 performed with the knee in neutral, varus or valgus alignment. The model outputs were

96 validated by comparing experimental and model-predicted tibio-femoral motion and ligament

97 length changes. To our knowledge, this is the first study to both simulate and validate the impact

98 of implant alignment on kinematics and ligament length changes as predicted by computer

99 models.

100 **4. Methods**

101 **4.1. Experimental data collection**

102 **4.1.1. Specimen preparation and imaging**

103 Three cadaveric knee specimens were used for squat simulations in a dynamic knee simulator

104 system. The methodology of the specimen preparation was similar to the workflow described

105 by Victor et al. [14]. The study protocol was approved by the local Ethics Committee.

106 After thawing the fresh frozen specimens, full leg T1-weighted opposed-phase spoiled gradient

107 echo magnetic resonance imaging (MRI) scans were obtained using a 3T scanner (Ingenia,

108 Philips Healthcare) to visualise soft tissues. The slice thickness was 2 mm and all slices had an

109 in plane resulotion of 0.9 mm x 0.9 mm. Subsequently, frames (Medtronic, MN, USA) with

4

reflective spherical markers were rigidly attached to femur, tibia and patella. Each frame carried 4 markers, which were 6 mm in diameter. The femoral frame was inserted within 21 cm from the joint line, the tibial frame within 18 cm from the joint line and the patellar frame was inserted onto the patella. To allow accurate three-dimensional motion tracking, a six-camera motion capture system (Vicon MX40, Oxford, UK) was used. The optical markers could accurately be located on the pre-operative and post-operative computed tomography (CT) scans.

Volumetric CT scans of the full lower leg with the attached markers were obtained on a dual-source multidetector CT scanner (SOMATOM Definition Flash, Siemens), equipped with two 64-detector row units, using a slice thickness of 0.75 mm and a pitch of 0.8 mm/rev. The images were processed in Mimics v. 17.0 (Materialise, Leuven, Belgium) to construct the bone models of femur, tibia and patella. These bone geometries were used to identify bony landmarks.

Next, the hip and foot were removed from the full leg, with a femoral cut 32 cm proximal of the joint line and a tibial cut 28 cm distal from the joint line. The quadriceps muscle was dissected and its preserved tendon was fixed into a clamp. In addition, the semitendinosus together with the semimembranosus muscle, as well as the biceps femoris muscle were dissected and suture wires were attached to the preserved tendons. The proximal femur and distal tibia were then embedded in aluminium containers, preserving the physiologic alignment in the coronal plane and parallel with the container in the sagittal plane.

Two extensometers (MTS, Eden Prairie, MN, USA) were sutured to the medial and lateral collateral ligaments by an experienced surgeon. The fixation of the extensometers was centred over the joint line, on an unloaded and fully extented knee [15]. During the measurements, ligament length change relative to the extended knee was calculated using the formula $\varepsilon = (L - L_r)/L_r$, where $L$ was the instantaneous length of the extensometer arms connected to the ligament and $L_r$ was the reference length at full extension.

### 4.1.2. Total knee replacement and imaging

An experienced surgeon (HD) performed the total knee arthroplasty on each specimen using a posterior-stabilised total knee arthroplasty (Performance, Biomet Inc., Warsaw, IN, USA). In addition to the tibial implant placed with standard alignment instrumentation, two variations of the tibial insert were designed through additive manufacturing. These variations were able to artificially simulate a TKA coronal malalignment by their built-in varus or valgus design. The inserts were modelled so that the central height was preserved while making one side thicker and the other side thinner than the neutral insert. For each specimen, three squat trials were performed. Specimen 1 underwent squats with neutral insert, 5° varus insert and 5° valgus insert. Specimen 2 and 3 underwent squats with neutral insert, 3° varus insert and 3° valgus insert. The tibial insert thickness for specimen 2 and 3 was smaller, leading to a smaller varus and valgus angle due to design limitations. The valgus insert squat of specimen 3 is not shown in the results since the quadriceps ruptured during the last experiment.

After the trials, post-operative CT scans were made with the optical markers still attached on the same scanner as the pre-operative scans, allowing to accurately document the implant position.

### 4.1.3. Knee simulator set-up

The specimens were mounted onto a dynamic knee simulator system, based on the Oxford rig [16]. This mechanical system permits six degrees-of-freedom (DOFs) for both the tibio-femoral and the patello-femoral joint. The femoral container was connected to an artificial hip assembly and the tibial container to an artificial ankle assembly. The quadriceps clamp was connected to an actuator that could apply a variable quadriceps load. Both hamstring wires were connected with constant-force springs of each 50 N (Type KKF 8077, Lesjöfors, Karlstad, Sweden). The hip assembly could slide vertically and flex and extend, the ankle assembly allowed rotation in

158 all three directions and translated medio-laterally. Sensors detected the quadriceps force, ankle

159 force and relative hip height and these real-time data were processed in a closed feedback

160 system (LabVIEW, National Instruments, Texas, USA), allowing the performance of a squat

161 motion by moving the hip assembly and applying a variable quadriceps force to induce a

162 vertical ankle force of 111 N. The quadriceps load increased during knee flexion, starting from

163 a few hundred Newton at the beginning of the experiment and the load could go up to 2000 N

164 at deep knee bend. A full squat motion began around 30-40° knee flexion and went up to 110-

165 120°. The squat did not begin at full extension to prevent hyperextension [14].

166 Six infrared emitting cameras (MX40, Vicon, Oxford, UK) tracked the reflecting light from the

167 rigidly attached optical markers on femur, tibia and patella at a sampling frequency of 100 Hz.

168 This provided us an accurate measurement of the knee joint motion during squat. Throughout

169 knee flexion, the three-dimensional (3D) coordinates of the passive markers were tracked and

170 the relative position of all the important landmarks on femur and tibia were computed. The

171 distance between the ligament insertion points on femur and tibia or fibula was used as the

172 ligament length at any given position in the flexion arc of the knee joint.

173 **4.2. Computational model definition**

174 **4.2.1. Subject-specific knee model set-up**

175 The experimental set-up was implemented into the AnyBody Modeling System 6.0.5 (AnyBody

176 Technology A/S, Denmark). The knee model consisted of the subject-specific bone geometry

177 segmented from CT scans in Mimics 17.0 (Materialise N.V., Leuven, Belgium). The implant

178 position was determined by the post-operative CT scans. The contact between femoral and tibial

179 implant and between femoral implant and patella was modelled using a rigid-rigid STL-based

180 contact model. The contact forces were computed based on the penetration depth, $d_i$, of a vertex

7

181  into the opponent surface. The penetration volume $V_i$ was approximated by the multiplication

182  of the penetration depth and the opponent triangle area $A_i$, so that for the $i$th vertex

$$V_i = A_i d_i \qquad (1)$$

183  The direction of the contact force was determined by the normal of the triangle and the contact

184  force magnitude for each contributing element was computed using a linear force law between

185  the penetration volume and the pressure module $P$

$$F_i = PV_i \qquad (2)$$

186  A pressure module of 4.6 GN/m$^3$ was used, based on previous tests where the trade-off between

187  the penetration depth and the numerical issues of solving contact between two surfaces with

188  high stiffness was investigated [10].

189  Four ligaments were defined: proximal and distal part of the medial collateral ligament (MCL),

190  lateral collateral ligament (LCL), medial patello-femoral ligament (MPFL) and lateral

191  epicondylo-patellar ligament (LEPL). The insertions were estimated based on an anatomical

192  atlas using the specimen's bony landmarks and two insertion sites of the MCL proximally and

193  distally on the tibia were identified (MCLprox and MCLdist) [14]. Ligaments were represented

194  as non-linear line segments that wrap over analytical surfaces approximating the relevant

195  geometries. One cylinder was placed medially on the tibia to allow the MCLdist to wrap around

196  the medial tibial condyle and another cylinder was fitted to the femoral implant to prevent the

197  quadriceps muscle from penetrating the implant during deep flexion. Two ellipsoids were

198  introduced to wrap the MPFL and LEPL around the femoral condyles (Figure 1).

199  Ligament force was modelled with the following force-displacement relationship [17]

$$f = \begin{cases} 1/4 k\varepsilon^2/\varepsilon_l & 0 \le \varepsilon \le 2\varepsilon_l \\ k(\varepsilon - \varepsilon_l) & \varepsilon > 2\varepsilon_l \\ 0 & \varepsilon < 0 \end{cases} \qquad (3)$$

200  where $f$ is the tensile force, $k$ the ligament stiffness, $\varepsilon_l$ the linear strain limit set at 0.03 [18]

201  and $\varepsilon$ the strain calculated with the ligament length $L$ and its zero-load length $L_0$ using the

202  equation $\varepsilon = (L - L_0)/L_0$. The zero-load length $L_0$ was computed using the following

203  definition:

$$L_0 = L_r/(\epsilon_r + 1) \qquad (4)$$

204  in which $L_r$ is the ligament reference length and $\epsilon_r$ the reference strain. The stiffness and

205  reference strain of MCL and LCL were based upon values given by Blankevoort and Huiskes

206  and can be found in Table 1 [17]. The ligament reference lengths were computed with the intact

207  knee in full extension. Not much information is available regarding the stiffness and reference

208  strain of the patellar ligaments MPFL and LEPL. The MPFL is the primary restraint to lateral

209  patellar displacement and lateral soft-tissues contribute less to the overall stability [19].

210  Accordingly, MPFL stiffness was chosen in the same range of MCL and LCL and lower values

211  were attributed to LEPL. Since patellar ligaments are tightest in full extension and slacken with

212  flexion, positive reference strain values were assigned in the same range of MCL and LCL [19].

213  Both MPFL and LEPL were represented by three line segments and their parameter values are

214  shown in Table 1.

215  To compare the model output to the local extensometer length changes, the reported model

216  ligament length changes were calculated using the formula $\varepsilon_{model} = (L - L_r)/L_r$. Additional

217  to the extensometer length changes, kinematic based ligament length changes were measured

218  by tracking the length changes of the ligament line segment during the experimental motion

219  compared to the length at full extension.

220  The simulation mimicked the experimental set-up, such that the same force to the quadriceps

221  tendon was applied and the same vertical motion of the hip assembly was generated. Figure 2

222  shows how the model was constrained during the simulation. The hip assembly could move up

223    and down and flex and extend. The ankle assembly could rotate in all three directions and could

224    move medio-laterally. Consequently, this configuration provided the tibio-femoral joint with

225    all six DOFs. The patello-femoral joint was modelled with the assumption of a constant length

226    of the patellar tendon, while the three translational DOFs and the spin and tilt (patellar rotation

227    around respectively the anterior-posterior axis and the proximal-distal axis) were solved by the

228    FDK solver. A simple linear torsional spring with spring constant of 100 Nm/rad was included

229    to ensure some stiffness in the patellar tilt direction during deep knee flexion when the patellar

230    ligaments were slack.

231    **4.2.2. Force-dependent kinematics**

232    Knee kinematics were simulated using FDK, an extended inverse dynamics approach, which

233    simultaneously computes ligament forces and secondary joint motions [10]. This methodology

234    relies on an assumption of quasi-static force equilibrium in the secondary joint kinematics at

235    each time step during the analysis, eliminating the need for time integration. This assumption

236    of static equilibrium only applies to the FDK directions and the full dynamics in all other DOFs

237    are taken into account. This modelling approach is implemented into the AnyBody Modeling

238    System (AnyBody Technology, A/S, Aalborg, Denmark).

239    **4.3. Data analysis**

240    **4.3.1. Sensitivity study**

241    A sensitivity analysis was performed to investigate the influence of the tibio-femoral model

242    parameters on the output. The insertion points of three ligament line segments (MCLprox,

243    MCLdist and LCL) as well as the patellar tendon were moved from their reference position.

244    Since the attachment of these structures is known to lay on the bone surface, the attachments

245    were varied in a plane tangent to the bone surface.

246 From a study investigating the precision in locating landmarks on CT scans, an estimate of the

247 appropriate variability was made [14]. In the study, an intra-variability of around 1 mm and the

248 inter-variability was 3.5 mm or less was reported. Based on these results, a variation of 3.5 mm

249 was first chosen, representing a range of 7 mm.

250 Consequently, all ligaments insertions were varied from -3.5 mm to +3.5 mm in the anterior-

251 posterior and proximal-distal direction. The insertions of the patellar tendon were varied from

252 -3.5 mm to +3.5 mm in the medial-lateral and anterior-posterior direction. When one of the

253 insertion locations was changed, the reference ligament length was recalculated and updated

254 prior to the simulation.

255 In addition, the stiffness and reference strain of the three ligament line segments were varied,

256 each from +3.5% to -3.5% of their reference value. A total of 45 configurations were analysed

257 and the overview of these simulations can be found in Table 2.

**4.3.1. Metrics**

259 The tibio-femoral rotations were derived using the Grood and Suntay protocol and the

260 translations were reported in the tibial reference frame [20]. Positive values were assigned to

261 medial, anterior and proximal translations and to valgus and external tibial rotations. Each of

262 these trials show the downwards motion of a squat.

263 The differences between the experimental and simulation results were quantified using the

264 Root-Mean-Square-Error (RMSE) and the Pearson correlation coefficient with ρ categorized as

265 $\rho \leq 0.35$, $0.35 < \rho \leq 0.67$, $0.67 < \rho \leq 0.9$, $0.9 < \rho$ to be weak, moderate, strong or excellent

266 correlations[21,22]

**5. Results**

268  The computed tibio-femoral translations (Figure 3) and rotations (Figure 4) showed a good

269  agreement, predicting the proximal-distal, medial-lateral, anterior-posterior, varus-valgus,

270  internal-external motions with an average RMSE of respectively 1.0 mm, 1.2 mm, 2.7 mm, 0.7°

271  and 2.3°. The average Pearson correlation coefficient for the aforementioned motions was 1.00,

272  0.38, 0.85, 0.93 and 0.95, showing strong or excellent correlations except for the medial-lateral

273  motion. This lower correlation is caused by the low order of magnitude of this motion. An

274  overview of the kinematic RMSE and Pearson correlation coefficient for all trials for each

275  cadaver can be found in Table 3.

276  Additionally, tibio-femoral motion can be more intuitively analysed when the 3D motion is

277  projected onto a two-dimensional (2D) plane. Figure 5 shows the projected tibio-femoral

278  kinematics during squat. Because of the clinical importance of rotational movement, the

279  projection plane of choice was the tibial horizontal plane. This plane is defined as the plane

280  perpendicular to the tibial mechanical axis and comprises the line connecting the tibial condyle

281  centres. The projections of the centres of the medial and lateral femoral condyles onto the tibial

282  horizontal plane were presented for different flexion angles, namely 40°, 60°, 80° and 100°.

283  An overview of the ligament length change RMSE and Pearson correlation coefficient for all

284  trials for each specimen can be found in Table 4. The lateral extensometer length change was

285  compared to the model LCL length change and the medial extensometer length change was

286  compared to the model MCLdist length change. The average RMSE was 2.7% for MCLdist and

287  4.0% for LCL and the average Pearson correlation coefficient was 0.96 and 0.74 for MCLdist

288  and LCL respectively. Figure 6 depicts the predicted subject-specific model length changes

289  compared to the kinematic based experimental length changes for all conditions. The average

290  RMSE was 0.9% for MCLdist and 2.5% for LCL and the average Pearson correlation

291  coefficient was 0.99 and 0.98 for MCLdist and LCL respectively.

292   Figure 7 shows the results of the sensitivity study for the three specimens for the neutral insert

293   trial. The translations were the least sensitive to changes in model parameters. The largest

294   changes can be found in internal-external rotation and ligament length changes, presenting

295   changes up to 3.8° in the maximum internal tibial rotation at the end of the simulation, and up

296   to 6.4% in the absolute ligament length change at the end of the simulation. The perturbed

297   simulations of specimen 2 failed to solve if MCL was less strained, hence we removed these

298   failed output resulting in a smaller shaded area for MCL.

299   **6. Discussion**

300   The motivation of this work was to develop a computational efficient subject-specific model

301   that can predict the relative impact of different implant configurations on kinematics and

302   ligament length change patterns. A validation was performed using *in vitro* kinematics and

303   ligament length changes of different component alignments for three different subjects.

304   The results showed that the kinematics can accurately be predicted, showing an average RMSE

305   of less than 2.7 mm and 2.3° for translations and rotations. The largest RMSE was for anterior-

306   posterior translation. The model consistently underestimated the anterior position of the femur

307   with respect to the tibia during the beginning of the squat, indicating that some anterior-

308   posterior stiffness is missing. In reality, the knee joint is surrounded by the joint capsule

309   membrane, which is lacking in the model. Overall, the kinematics showed an excellent

310   correlation and small RMSE for the three subjects during the three different alignment

311   conditions. The motions are comparable in trend and in magnitude with the results of Baldwin

312   et al., who validated a finite element (FE) knee model with a posterior-stabilised implant for

313   three cadaveric knees inside a mechanical rig [23]. The ligament parameters and attachment

314   sites were optimised by minimising differences between model-predicted and experimental

315   kinematics. They noted average RMSE of less than 1.8 mm and 2.2° for translations and

316   rotations respectively. Without ligament parameter optimisation, our model achieved similar

13

317 results. Moreover, the predicted kinematics after component malrotation showed comparable

318 RMSE.

319 To evaluate the differences caused by malalignment, the different rows for one specimen can

320 be compared in Figure 5. Valgus malalignment resulted in a more externally rotated starting

321 position of the tibia, whereas varus malalignment caused a slightly more internally rotated tibia

322 compared to the neutral alignment. This presents a direct link to ligament behaviour, since the

323 collateral ligaments are known to be important stabilisers. MCL was more strained in valgus

324 and acts as a restraint to tibial internal rotation, LCL experienced more strain in varus,

325 increasing the restraint to tibial external rotation [24].

326 Next to changes introduced by coronal malalignment, the inter-specimen variability influenced

327 the kinematics as well. Even though the contact geometry was identical for all specimens,

328 different kinematic behaviour between the specimens can be seen, in particular with respect to

329 the amount of anterior-posterior translation. Nevertheless, the model was able to closely match

330 the experimental kinematics for each specimen. All specimens showed posterior femoral

331 rollback laterally, abnormal anterior femoral translation medially was present for Specimen 1.

332 Similar inter-specimen variability of kinematics after TKA was also seen *in vivo* [23].

333 Abnormal anterior motion was mostly attributed to lack of PCL and unbalanced collateral

334 ligaments [26]. This explanation seems plausible, since anterior translation was mostly present

335 for varus malalignent of Specimen 1, where 5° of malalignment was introduced as opposed to

336 the 3° of malalignment in Specimen 2 and 3. During varus malrotation, MCL was more slack,

337 resulting in more instability.

338 From the sensitivity study, it is clear that the ligament length change is sensitive to the model

339 parameters. However, the trend of ligament behaviour as a function of implant alignment can

340 be captured by the model. When comparing the extensometer length changes to the model, an

341 excellent average correlation of 0.96 and RMSE of 2.7% was seen for MCL, while LCL had a

14

342     strong average correlation of 0.74 and an RMSE of 4.0%. Extensometer length changes are

343     local length changes measured at the mid-region of the ligament, whereas the reported model

344     length changes show average length changes between the insertion points. Hence, additional to

345     the local extensometer length changes, the kinematic based ligament length changes were

346     reported, since experimental ligament length changes are often described using the length

347     between the ligament insertions during the reproduced motion [27]. In our study, these

348     kinematic based length changes showed a strong to excellent correlation and the average RMSE

349     is below 2.5% for all ligament segments. The local extensometer and kinematic based

350     experimental length changes agreed well for MCL, while showing larger deviations for LCL,

351     indicating that the simple ligament model cannot fully represent the variable behaviour of the

352     LCL.

353     This study investigated the relative behaviour of ligament length changes when varying implant

354     alignment. When introducing the different configurations for the tibial insert, the model and

355     kinematic based experimental strains showed an analogous behaviour. This behaviour is

356     consistent with the results of Delport et al. [28]. They reported that both for the neutral aligned

357     as for the varus or valgus configurations, MCL as well as LCL remained isometric in the

358     beginning of the squat and then started to relax. In addition, the relative relationship between

359     the varus, neutral and valgus alignment corresponds well to our results, resulting in more MCL

360     strain and less LCL strain for valgus malalignment and the other way around for varus

361     malalignment.

362     The use of mechanical knee simulators in validation studies is a cost-effective and controlled

363     method to mimic real-life conditions. However, this set-up differs from the actual physiologic

364     loading condition, for instance keeping the hip fixed over the ankle and the constant hamstrings

365     load. Despite this artificial representation, the knee motions agree well with *in vivo* motions,

366     supporting the use of such rigs as an intermediate step towards clinical application. Two studies

of Victor et al. looked at knee motions, one in a mechanical rig [14] and one in real patients [29]. The *in vitro* study with cadaver knees in a mechanical rig showed mean ranges of motion for tibial rotation and for posterior translation of the medial and lateral femoral condyle of respectively 9.7°, 12.9 mm and 16.3 mm for a PS implant [14]. In the second study, *in vivo* kinematics were measured in TKA patients during deep knee bend with the help of dynamic fluoroscopy [29]. The average range of the aforementioned motions was 10.8°, 14 mm and 23 mm.

The results of the current study need to be seen within the light of the following limitations. The same implant type was used in all three specimens, which meant sacrificing the cruciate ligaments. Cruciate-retaining implants were not tested. Furthermore, the reported extensometer values show only the ligament length changes at the location where the extensometer is sutured. However, ligaments show different length change behaviour at different locations. Ligament model parameters were based on values from literature to demonstrate the generic workflow. However, it is known that ligament zero-load lengths are sensitive parameters in computational models but difficult to measure [30–32]. Other studies often optimize these zero-load lengths until the rotational knee behaviour matches the experimental data [33]. Finally, only coronal implant position variation is modelled here. In future work, we plan to investigate other implant configuration such as joint line variation.

In summary, this work presented a model-based and experimental evaluation of the prediction of knee kinematics and ligament length changes for three different subjects following TKA. Malalignment was introduced and the associated changes in knee kinematic and ligament length change patterns could be predicted well by the model. Despite the identical implant geometry, inter-specimen differences were both experimentally observed and predicted by the subject-specific model. This validation study is a first, necessary step towards the clinical application of musculoskeletal models. Model credibility to predict component malalignment was assured

16

392    in this work and the current results support the potential of subject-specific musculoskeletal

393    modelling to aid surgeons in deciding the optimal implant configuration for a patient.

394    **Conflict of interest**

395    The authors declare that they have no conflicts of interest.

396    **7. Acknowledgments**

401

402

403

404

405

406

407

408

409

410

411

412

**8. References**

[1]   Griffin FM, Insall JN, Scuderi GR. Accuracy of soft tissue balancing in total knee arthroplasty. J Arthroplasty 2000;15:970–3.

[2]   Abdel MP. Measured resection versus gap balancing for total knee arthroplasty. Clin Orthop Relat Res 2014;472:2016–22.

[3]   Fregly BJ, Besier TF, Lloyd DG, Delp SL, Banks SA, Pandy MG, et al. Grand challenge competition to predict in vivo knee loads. J Orthop Res 2012;30:503–13.

[4]   Amiri S, Cooke D, Kim IY, Wyss U. Mechanics of the passive knee joint. Part 2: interaction between the ligaments and the articular surfaces in guiding the joint motion. Proc Inst Mech Eng Part H J Eng Med 2007;221:821–32.

[5]   Wilson DR, Feikes JD, O'Connor JJ. Ligaments and articular contact guide passive knee flexion. J Biomech 1998;31:1127–36.

[6]   Hast MW, Piazza SJ. Dual-joint modeling for estimation of total knee replacement contact forces during locomotion. J Biomech Eng 2013;135:021013.

[7]   Thelen DG, Won Choi K, Schmitz AM. Co-Simulation of Neuromuscular Dynamics and Knee Mechanics During Human Walking. J Biomech Eng 2014;136:021033.

[8]   Guess TM, Stylianou AP, Kia M. Concurrent prediction of muscle and tibiofemoral contact forces during treadmill gait. J Biomech Eng 2014;136:021032.

[9]   Andersen MS, Damsgaard M, Rasmussen J. Force-dependent kinematics : a new analysis method for non-conforming joints. 13th Bienn. Int. Symp. Comput. Simul. Biomech., 2011.

[10]  Marra MA, Vanheule V, Rasmussen J, Verdonschot NJJ, Andersen MS. A Subject-Specific Musculoskeletal Modeling Framework to Predict in Vivo Mechanics of Total Knee Arthroplasty. J Biomech Eng 2014;137:020904.

[11]  Thompson JA, Hast MW, Granger JF, Piazza SJ, Siston RA. Biomechanical effects of total knee arthroplasty component malrotation: A computational simulation. J Orthop Res 2011;29:969–75.

[12]  Chen Z, Wang L, Liu Y, He J, Lian Q, Li D, et al. Effect of component mal-rotation on knee loading in total knee arthroplasty using multi-body dynamics modeling under a simulated walking gait. J Orthop Res 2015;33:1287–96.

455 [13] Werner FW, Ayers DC, Maletsky LP, Rullkoetter PJ. The effect of valgus/varus
456 malalignment on load distribution in total knee replacements. J Biomech 2005;38:349–
457 55.
458

459 [14] Victor J, Bellemans J. A comparative study on the biomechanics of the native human
460 knee joint and total knee arthroplasty. Dep Orthop Fac Med 2009;PhD.
461

462 [15] Delport H, Labey L, De Corte R, Innocenti B, Vander Sloten J, Bellemans J. Collateral
463 ligament strains during knee joint laxity evaluation before and after TKA. Clin Biomech
464 2013;28:777–82.
465

466 [16] Zavatsky AB. A kinematic-freedom analysis of a flexed-knee-stance testing rig. J
467 Biomech 1997;30:277–80.
468

469 [17] Blankevoort L, Huiskes R. Ligament-bone interaction in a three-dimensional model of
470 the knee. J Biomech Eng 1991;113:263–9.
471

472 [18] Butler DL, Kay MD, Stouffer DC. Comparison of material properties in fascicle-bone
473 units from human patellar tendon and knee ligaments. J Biomech 1986;19:425–32.
474

475 [19] Amis AA, Firer P, Mountney J, Senavongse W, Thomas NP. The anatomy and
476 reconstruction of the medial patellofemoral ligament. Knee 2003;10:215–20.
477

478 [20] Grood ES, Suntay WJ. A Joint Coordinate System for the Clinical Description of Three-
479 Dimensional Motions: Application to the Knee. J Biomech Eng 1983;105:136–44.
480

481 [21] Taylor R. Interpretation of the Correlation Coefficient: A Basic Review. J Diagnostic
482 Med Sonogr 1990;6 :35–9.
483

484 [22] Fluit R, Andersen MS, Kolk S, Verdonschot N, Koopman HFJM. Prediction of ground
485 reaction forces and moments during various activities of daily living. J Biomech
486 2014;47:2321–9.
487

488 [23] Baldwin MA, Clary CW, Fitzpatrick CK, Deacy JS, Maletsky LP, Rullkoetter PJ.
489 Dynamic finite element knee simulation for evaluation of knee replacement mechanics.
490 J Biomech 2012;45:474–83.
491

492 [24] Athwal KK, Hunt NC, Davies AJ, Deehan DJ, Amis A a. Clinical biomechanics of
493 instability related to total knee arthroplasty. Clin Biomech 2014;29:119–28.
494

495 [25] Dennis D a, Komistek RD, Colwell CE, Ranawat CS, Scott RD, Thornhill TS, et al. In
496 Vivo Anteroposterior Femorotibial Translation of Total Knee Arthroplasty: A

497     Multicenter Analysis. Clin Orthop Relat Res 1998;353:47–57.
498

499     [26]    Cromie MJ, Siston RA, Giori NJ, Delp SL. Posterior cruciate ligament removal
500             contributes to abnormal knee motion during posterior stabilized total knee arthroplasty.
501             J Orthop Res 2008;26:1494–9.
502

503     [27]    Park SE, DeFrate LE, Suggs JF, Gill TJ, Rubash HE, Li G. Erratum to "The change in
504             length of the medial and lateral collateral ligaments during in vivo knee flexion". Knee
505             2006;13:77–82.
506

507     [28]    Delport H, Labey L, Innocenti B, De Corte R, Vander Sloten J, Bellemans J. Restoration
508             of constitutional alignment in TKA leads to more physiological strains in the collateral
509             ligaments. Knee Surgery, Sport Traumatol Arthrosc 2015;23:2159–69.
510

511     [29]    Victor J, Mueller JKP, Komistek RD, Sharma A, Nadaud MC, Bellemans J. In Vivo
512             Kinematics after a Cruciate-substituting TKA. Clin Orthop Relat Res 2010;468:807–14.
513

514     [30]    Baldwin MA, Laz PJ, Stowe JQ, Rullkoetter PJ. Efficient probabilistic representation of
515             tibiofemoral soft tissue constraint. Comput Methods Biomech Biomed Engin
516             2009;12:651–9.
517

518     [31]    H. Bloemker K. Computational Knee Ligament Modeling Using Experimentally
519             Determined Zero-Load Lengths. Open Biomed Eng J 2012;6:33–41.
520

521     [32]    Beillas P, Lee SW, Tashman S, Yang KH. Sensitivity of the tibio-femoral response to
522             finite element modeling parameters. Comput Methods Biomech Biomed Engin
523             2007;10:209–21.
524

525     [33]    Pandy MG, Sasaki K, Kim S. A Three-Dimensional Musculoskeletal Model of the
526             Human Knee Joint. Part 1: Theoretical Construction. Comput Methods Biomech Biomed
527             Engin 1997;1:87–108.
528


529

## 9. Tables

Table 1: Reference strain ($\epsilon_r$) and stiffness ($k$) values adapted from Blankevoort and Huiskes [17]. The literature values were slightly adapted since our model has two MCL bundles and one LCL bundle while their model has three bundles for both MCL and LCL. The stiffness was redistributed according to the number of bundles, MCL reference strain could be copied and the LCL reference strain was copied such that the bundle was tensioned in full extension. Both MPFL and LEPL consisted of three bundles and the reported parameter values were assigned to each bundle.

|  | MCL | LCL | MPFL | LEPL |
|---|---|---|---|---|
| $\epsilon_r$ | 0.04 | 0.08 | 0.08 | 0.06 |
| $k$ (N) | 4125 | 6000 | 2000 | 1000 |

Table 2: Summary of the different configurations of the sensitivity study. For each configuration, only one model parameter was perturbed while all other model parameters were kept constant.

| Component | Measure | Low value | Initial value | High value |
|---|---|---|---|---|
| LCL tibia | Ant-pos | -3.5 mm | reference | +3.5 mm |
| | Prox-dis | -3.5 mm | reference | +3.5 mm |
| LCL femur | Ant-pos | -3.5 mm | reference | +3.5 mm |
| | Prox-dis | -3.5 mm | reference | +3.5 mm |
| MCLprox tibia | Ant-pos | -3.5 mm | reference | +3.5 mm |
| | Prox-dis | -3.5 mm | reference | +3.5 mm |
| MCLprox femur | Ant-pos | -3.5 mm | reference | +3.5 mm |
| | Prox-dis | -3.5 mm | reference | +3.5 mm |
| MCLdist tibia | Ant-pos | -3.5 mm | reference | +3.5 mm |
| | Prox-dis | -3.5 mm | reference | +3.5 mm |
| MCLdist femur | Ant-pos | -3.5 mm | reference | +3.5 mm |
| | Prox-dis | -3.5 mm | reference | +3.5 mm |
| Patellar tendon tibia | Med-lat | -3.5 mm | reference | +3.5 mm |
| | Prox-dis | -3.5 mm | reference | +3.5 mm |
| Patellar tendon patella | Med-lat | -3.5 mm | reference | +3.5 mm |
| | Prox-dis | -3.5 mm | reference | +3.5 mm |
| LCL | k | 5790 N | 6000 N | 6210 N |
| | $\varepsilon_r$ | 0.045% | 0.08% | 0.115% |
| MCLprox | k | 3980N | 4125 N | 4270 N |
| | $\varepsilon_r$ | 0.005% | 0.04% | 0.075% |
| MCLdist | k | 3980N | 4125 N | 4270 N |
| | $\varepsilon_r$ | 0.005% | 0.04% | 0.075% |

Table 3: Comparison of measured and computed kinematics using RMSE and Pearson correlation coefficient ρ. Proximal-distal (PD), medial-lateral (ML), anterior-posterior (AP), varus-valgus (VV) and internal-external (IE) motions are shown.

| | RMSE | | | | | ρ | | | | |
|---|---|---|---|---|---|---|---|---|---|---|
| | PD (mm) | ML (mm) | AP (mm) | VV (°) | IE (°) | PD | ML | AP | VV | IE |
| Specimen 1 | | | | | | | | | | |
| Neutral | 1.34 | 1.50 | 2.43 | 0.67 | 2.00 | 1.00 | 0.40 | 0.69 | 0.89 | 0.94 |
| Varus | 1.53 | 1.16 | 2.26 | 0.61 | 1.97 | 1.00 | 0.79 | 0.66 | 0.79 | 0.99 |
| Valgus | 0.89 | 2.19 | 2.58 | 0.41 | 2.91 | 1.00 | -0.08 | 0.75 | 0.97 | 0.94 |
| Specimen 2 | | | | | | | | | | |
| Neutral | 0.47 | 0.89 | 2.95 | 0.80 | 2.65 | 1.00 | 0.00 | 0.91 | 0.93 | 0.92 |
| Varus | 0.44 | 0.65 | 2.18 | 1.26 | 3.23 | 1.00 | 0.88 | 0.94 | 0.99 | 0.93 |
| Valgus | 0.53 | 0.44 | 2.41 | 0.65 | 2.04 | 1.00 | 0.78 | 0.90 | 0.86 | 0.95 |
| Specimen 3 | | | | | | | | | | |
| Neutral | 1.38 | 0.93 | 3.26 | 0.45 | 1.94 | 0.99 | 0.43 | 0.97 | 1.00 | 0.97 |
| Varus | 1.52 | 1.82 | 3.13 | 0.75 | 1.58 | 0.99 | -0.16 | 0.95 | 1.00 | 0.97 |
| Average | 1.01 ± 0.45 | 1.20 ± 0.56 | 2.65 ± 0.38 | 0.70 ± 0.25 | 2.29 ± 0.53 | 1.00 ± 0.00 | 0.38 ± 0.39 | 0.85 ± 0.12 | 0.93 ± 0.07 | 0.95 ± 0.02 |

Table 4: Comparison of experimental and computed ligament length changes using RMSE and Pearson correlation coefficient ρ. Kinematic based length changes (Kin) and extensometer length changes (Ext) are shown.

| | RMSE | | | | ρ | | | |
|---|---|---|---|---|---|---|---|---|
| | MCL Ext (%) | MCL Kin (%) | LCL Ext (%) | LCL Kin (%) | MCL Ext | MCL Kin | LCL Ext | LCL Kin |
| Specimen 1 | | | | | | | | |
| Neutral | 1.88 | 0.87 | 3.45 | 3.26 | 0.98 | 0.99 | 0.25 | 0.99 |
| Varus | 4.64 | 1.11 | 1.99 | 3.44 | 0.97 | 0.99 | 0.28 | 0.97 |
| Valgus | 2.24 | 1.09 | 4.07 | 1.49 | 0.96 | 0.97 | 0.67 | 0.95 |
| Specimen 2 | | | | | | | | |
| Neutral | 2.08 | 0.44 | 4.97 | 1.74 | 0.99 | 1.00 | 0.95 | 0.97 |
| Varus | 2.03 | 0.76 | 4.05 | 2.25 | 0.94 | 0.99 | 0.99 | 0.98 |
| Valgus | 1.87 | 0.65 | 3.04 | 1.39 | 0.96 | 0.97 | 0.98 | 0.99 |
| Specimen 3 | | | | | | | | |
| Neutral | 2.83 | 1.27 | 5.92 | 2.73 | 0.93 | 0.99 | 0.87 | 0.98 |
| Varus | 3.95 | 1.10 | 4.73 | 3.82 | 0.92 | 0.99 | 0.92 | 0.98 |
| Average | 2.69 ±0.98 | 0.91 ±0.26 | 4.03 ±1.14 | 2.51 ±0.88 | 0.96 ±0.02 | 0.99 ±0.01 | 0.74 ±0.29 | 0.98 ±0.01 |

**Figure legends**

Figure 1: Illustration of the analytical surfaces that were fitted to the bone and implant geometries as wrapping surfaces. One cylinder was placed medially, allowing the MCLdist to wrap around the medial tibial condyle. Another cylinder was fitted to the femoral implant to prevent the quadriceps muscle from penetrating the implant in deep flexion. Two ellipsoids were introduced to wrap the MPFL and LEPL around the femoral condyles.

Figure 2: Illustration of the simulation of the mechanical rig inside AnyBody. The hip joint has 2 DOFs: vertical translation and flexion-extension. The ankle joint has 4 DOFs: all three rotations and medio-lateral translation. This configuration provides the tibio-femoral joint with all six DOFs. The patello-femoral joint was modelled with the assumption of a constant length for the patellar tendon and the other 5 DOF were solved using FDK.

Figure 3: Comparison of experimental and model tibio-femoral translations of the three specimens. Experimental (marker) and computed (line) proximal-distal (black/circles), medial-lateral (red/crosses) and anterior-posterior (blue/squares) translations are shown. The rows show the results for the different specimens, the columns show the results for the different configurations (varus insert, neutral insert and valgus insert).

Figure 4: Comparison of experimental and model tibio-femoral rotations of the three specimens. Experimental (marker) and computed (line) varus-valgus (black/circles) and internal-external (red/crosses) rotations are shown. The rows show the results for the different specimens, the columns show the results for the different configurations (varus insert, neutral insert and valgus insert).

Figure 5: 2D view of experimental (dotted lined) and model kinematics (full line) of the three specimens. The centres of the medial and lateral femoral condy

les are projected onto the tibial horizontal plane for different flexion angles (40°, 60°, 80° and 100°). The rows show the results for the different specimens, the columns show the results for the different configurations (varus insert, neutral insert and valgus insert). The top view of each specimen's left knee is depicted, with the anterior side pointing upwards.

Figure 6: Comparison of kinematic based experimental and model ligament length changes of the three specimens. Experimental (marker) and computed (line) MCLdist (black/circles) and LCL (red/crosses) strains are shown. The rows show the results for the different specimens, the columns show the results for the different configurations (varus insert, neutral insert and valgus insert).

Figure 7: The different output curves of the sensitivity analysis are shown as a shaded area on the figures. The first column shows translations, the second column rotations and the third and fourth column ligament length changes for the neutral configuration of each specimen (rows). The experimental measured data is shown in dotted line and the simulation with reference values in full line. For the translations, proximal-distal (red). medial-lateral (blue) and anterior-posterior (green) is shown. For the rotations, varus-valgus (red) and internal-external (blue) is depicted.
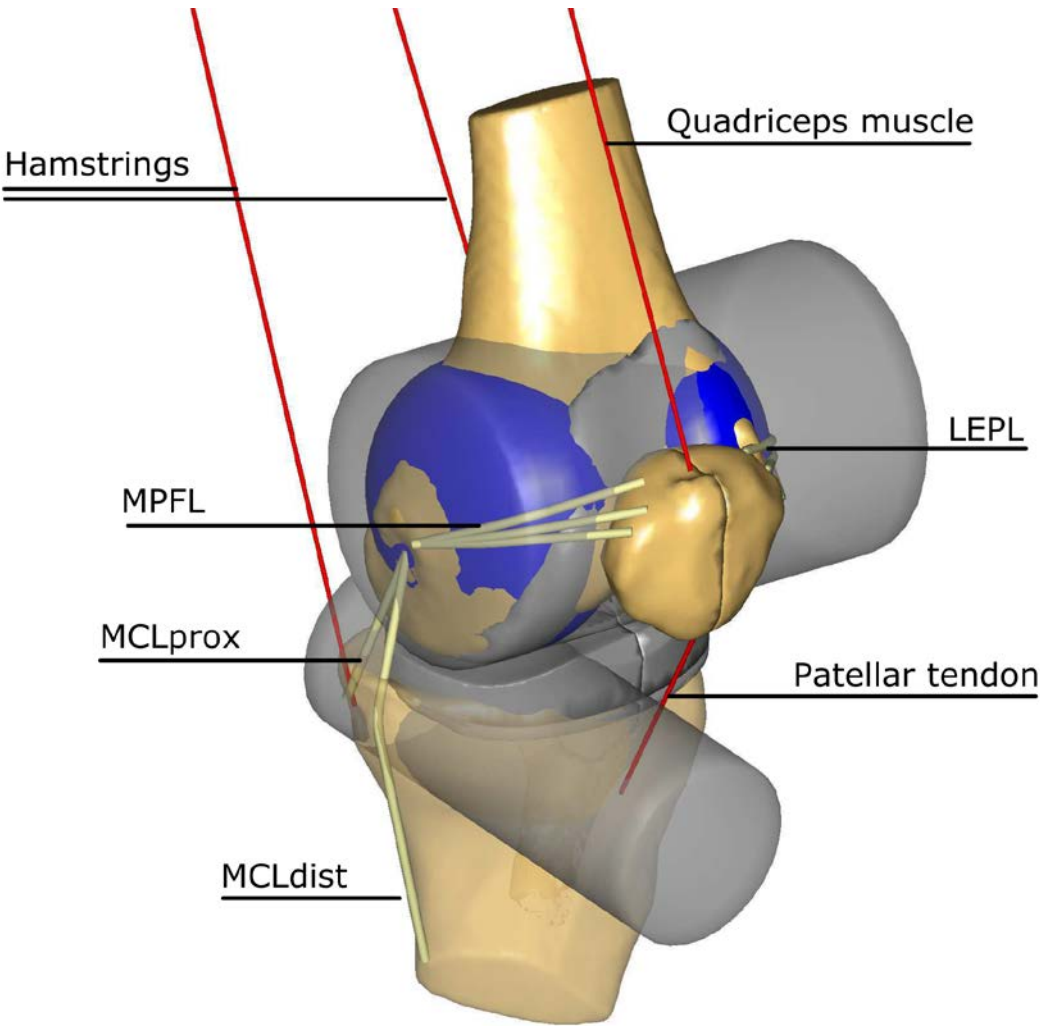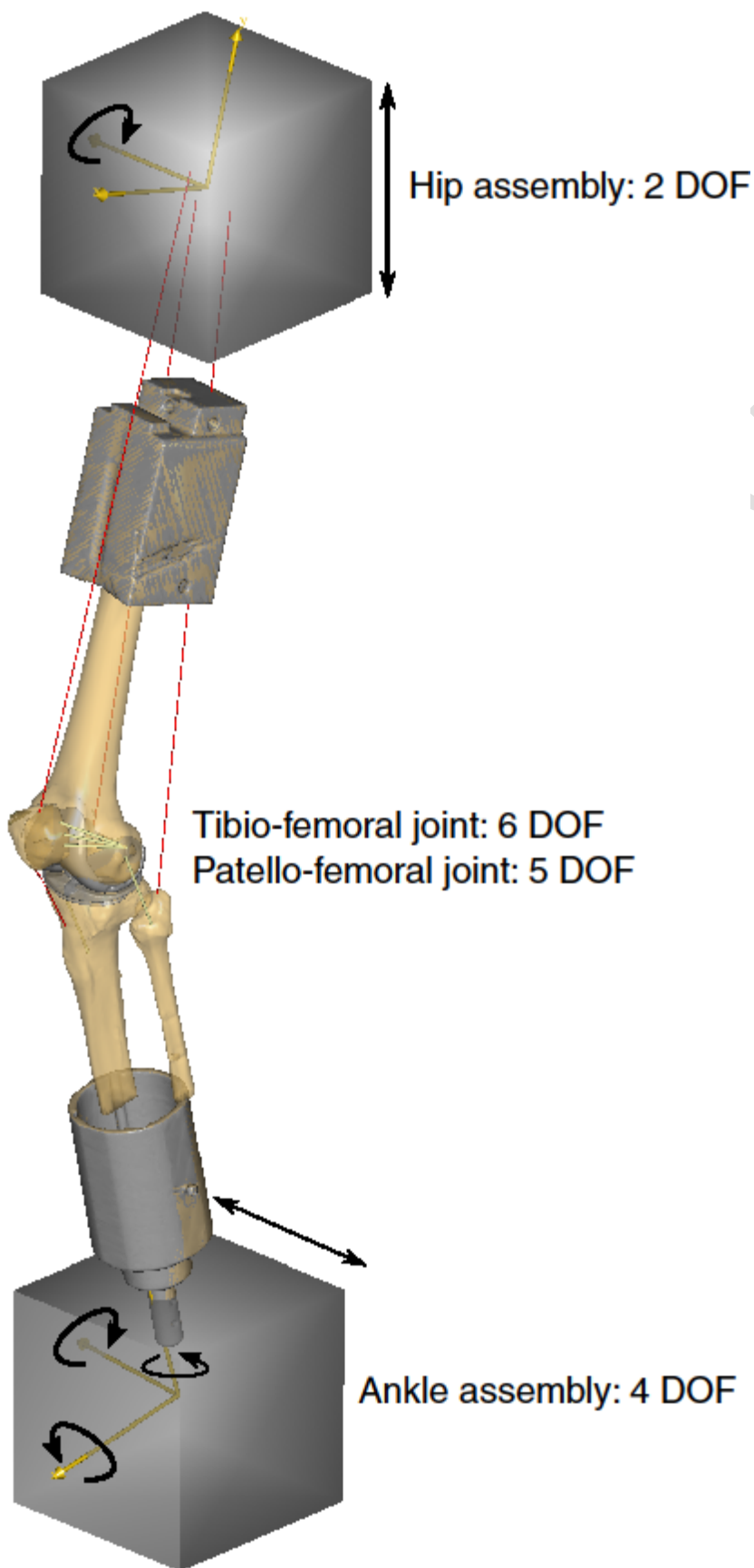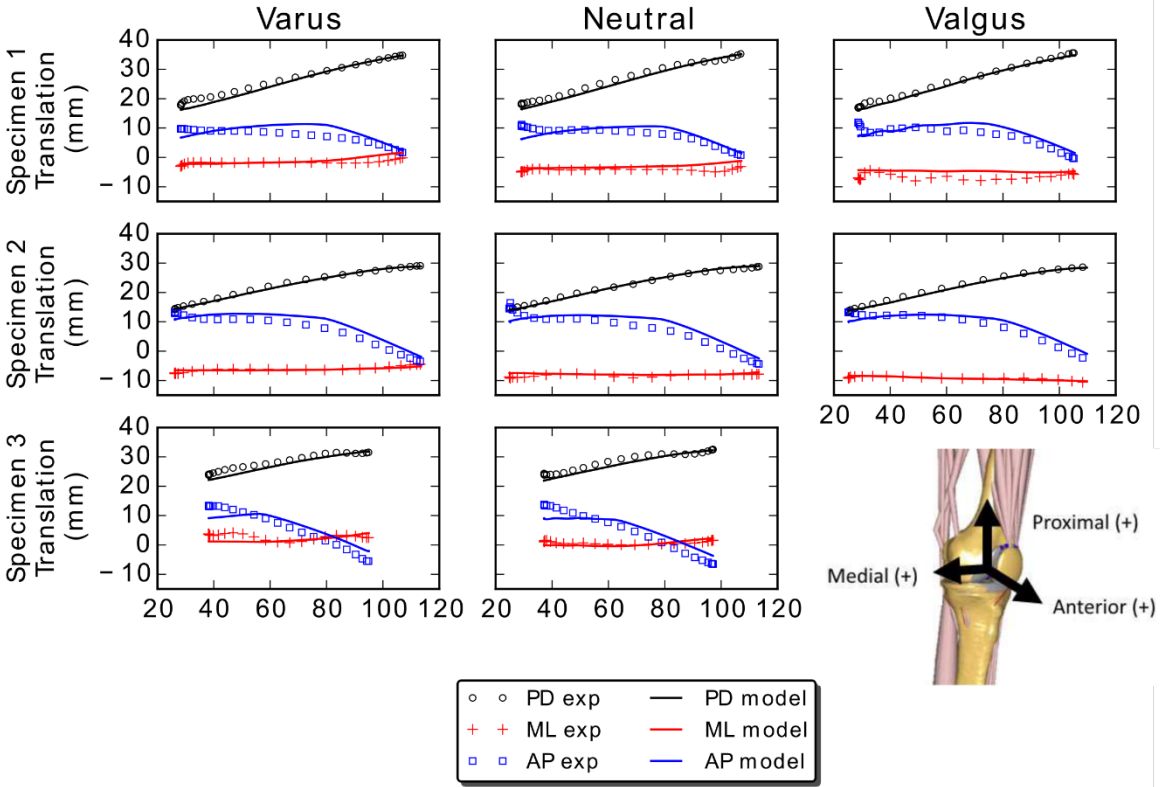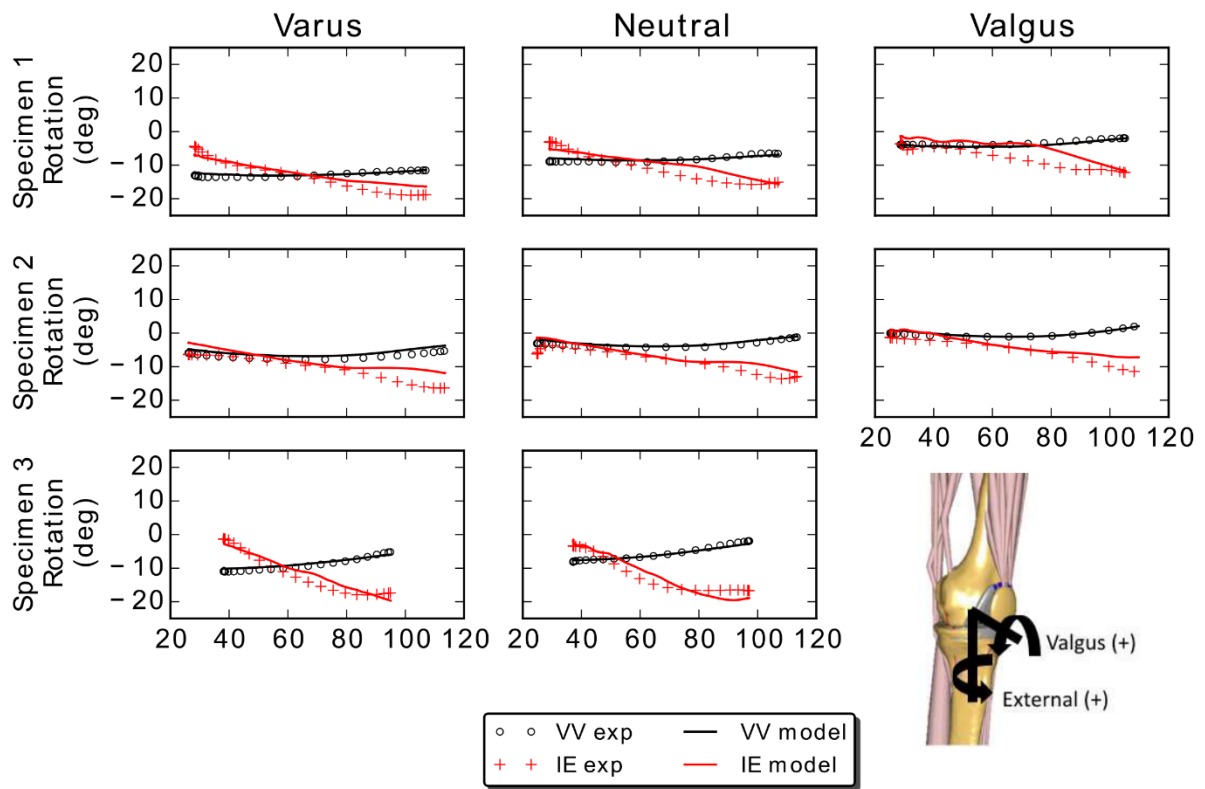
**Figure 1**

**Figure 2**



Hip assembly: 2 DOF

Tibio-femoral joint: 6 DOF
Patello-femoral joint: 5 DOF

Ankle assembly: 4 DOF

**Figure 3**

**Figure 4**

**Figure 5**



(a) Varus experiment

(b) Varus model

(c) Neutral experiment

(d) Neutral model

(e) Valgus experiment

(f) Valgus model

**Figure 6**

**Figure 7**